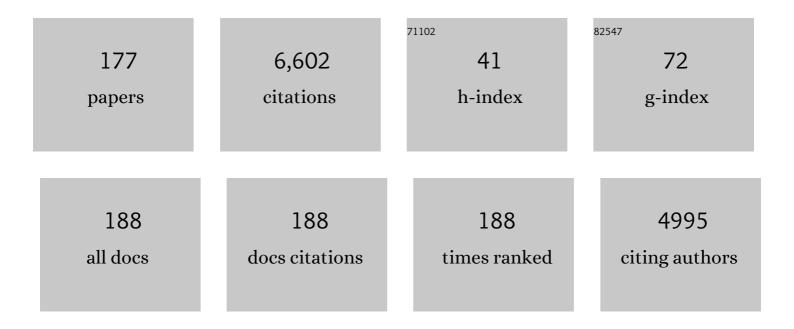
## Xiaoming Wang

List of Publications by Year in descending order

Source: https://exaly.com/author-pdf/1428166/publications.pdf Version: 2024-02-01



#	Article	IF	CITATIONS
1	GNSS-RS Tomography: Retrieval of Tropospheric Water Vapor Fields Using GNSS and RS Observations. IEEE Transactions on Geoscience and Remote Sensing, 2022, 60, 1-13.	6.3	10
2	Detecting heavy rainfall using anomaly-based percentile thresholds of predictors derived from GNSS-PWV. Atmospheric Research, 2022, 265, 105912.	4.1	17
3	A New Cumulative Anomaly-Based Model for the Detection of Heavy Precipitation Using GNSS-Derived Tropospheric Products. IEEE Transactions on Geoscience and Remote Sensing, 2022, 60, 1-18.	6.3	10
4	Deoxygenative Crossâ€Coupling of Aromatic Amides with Polyfluoroarenes. Angewandte Chemie - International Edition, 2022, 61, .	13.8	20
5	Long-Range and Short-Range Structures of Multimetallic Layered Double Hydroxides. Journal of Physical Chemistry C, 2022, 126, 5311-5322.	3.1	10
6	Weighted Mean Temperature Modelling Using Regional Radiosonde Observations for the Yangtze River Delta Region in China. Remote Sensing, 2022, 14, 1909.	4.0	5
7	Overcoming O–H Insertion to <i>Para</i> -Selective C–H Functionalization of Free Phenols: Rh(II)/Xantphos Catalyzed Geminal Difunctionalization of Diazo Compounds. ACS Central Science, 2022, 8, 581-589.	11.3	20
8	Histone methyltransferase Nsd2 ensures maternal–fetal immune tolerance by promoting regulatory T-cell recruitment. , 2022, 19, 634-643.		6
9	An Investigation of Near Real-Time Water Vapor Tomography Modeling Using Multi-Source Data. Atmosphere, 2022, 13, 752.	2.3	1
10	Efficient synthesis of β-substituted amines via combining deoxygenation of amides with photochemical organocatalysis. Cell Reports Physical Science, 2022, 3, 100955.	5.6	10
11	Dragon bones from the heavens: European explorations and early palaeontology in Zanda Basin of Tibet, retracing type locality of <i>Qurliqnoria hundesiensis</i> and <i>Hipparion</i> ( <i>Plesiohipparion</i> ) <i>zandaense</i> . Historical Biology, 2021, 33, 2216-2227.	1.4	6
12	Synthesis of Cyclic Amidines by Iridium-Catalyzed Deoxygenative Reduction of Lactams and Tandem Reaction with Sulfonyl Azides. Organic Letters, 2021, 23, 225-230.	4.6	26
13	An Improved Model for Detecting Heavy Precipitation Using GNSS-Derived Zenith Total Delay Measurements. IEEE Journal of Selected Topics in Applied Earth Observations and Remote Sensing, 2021, 14, 5392-5405.	4.9	20
14	As( <scp>iii</scp> ) adsorption–oxidation behavior and mechanisms on Cr( <scp>vi</scp> )-incorporated schwertmannite. Environmental Science: Nano, 2021, 8, 1593-1602.	4.3	7
15	A Type of Structurally Adaptable Aromatic Spiroketal Based Chiral Diphosphine Ligands in Asymmetric Catalysis. Accounts of Chemical Research, 2021, 54, 668-684.	15.6	61
16	Molecular-Scale Understanding of Sulfate Exchange from Schwertmannite by Chromate Versus Arsenate. Environmental Science & Technology, 2021, 55, 5857-5867.	10.0	35
17	A New Method for Determining an Optimal Diurnal Threshold of GNSS Precipitable Water Vapor for Precipitation Forecasting. Remote Sensing, 2021, 13, 1390.	4.0	9
18	An Improved and Privacy-Preserving Mutual Authentication Scheme with Forward Secrecy in VANETs. Security and Communication Networks, 2021, 2021, 1-12.	1.5	13

#	Article	IF	CITATIONS
19	Merging Electron Transfer with 1,2â€Metalate Rearrangement: Deoxygenative Arylation of Aromatic Amides with Arylboronic Esters. Angewandte Chemie, 2021, 133, 17225-17230.	2.0	5
20	Selective hydroboration of unsaturated bonds by an easily accessible heterotopic cobalt catalyst. Nature Communications, 2021, 12, 3813.	12.8	25
21	Merging Electron Transfer with 1,2â€Metalate Rearrangement: Deoxygenative Arylation of Aromatic Amides with Arylboronic Esters. Angewandte Chemie - International Edition, 2021, 60, 17088-17093.	13.8	27
22	Dirhodium(II)/Xantphos-Catalyzed Relay Carbene Insertion and Allylic Alkylation Process: Reaction Development and Mechanistic Insights. Journal of the American Chemical Society, 2021, 143, 11799-11810.	13.7	34
23	Fraction distribution of heavy metals and its relationship with iron in polluted farmland soils around distinct mining areas. Applied Geochemistry, 2021, 130, 104969.	3.0	29
24	Rate-Compatible Codes via Recursive BMST for Content-Sharing in Intelligent Vehicular Network. IEEE Transactions on Intelligent Transportation Systems, 2021, 22, 3929-3938.	8.0	0
25	H-BPin/KO <sup><i>t</i></sup> Bu Promoted Activation of Cobalt Salt to a Heterotopic Catalyst for Highly Selective Cyclotrimerization of Alkynes. Organic Letters, 2021, 23, 6925-6930.	4.6	4
26	Niâ€Catalyzed Regioselective Hydroarylation of 1â€Arylâ€1,3â€Butadienes with Aryl Halides. Chemistry - A European Journal, 2021, 27, 15903-15907.	3.3	10
27	A new zenith hydrostatic delay model for real-time retrievals of GNSS-PWV. Atmospheric Measurement Techniques, 2021, 14, 6379-6394.	3.1	6
28	Asymmetric Deoxygenative Alkynylation of Tertiary Amides Enabled by Iridium/Copper Bimetallic Relay Catalysis. Angewandte Chemie, 2021, 133, 26808-26813.	2.0	9
29	Asymmetric Deoxygenative Alkynylation of Tertiary Amides Enabled by Iridium/Copper Bimetallic Relay Catalysis. Angewandte Chemie - International Edition, 2021, 60, 26604-26609.	13.8	43
30	A neural network-based approach for the detection of heavy precipitation using GNSS observations and surface meteorological data. Journal of Atmospheric and Solar-Terrestrial Physics, 2021, 225, 105763.	1.6	16
31	Update China geodetic coordinate frame considering plate motion. Satellite Navigation, 2021, 2, .	8.6	7
32	Dinuclear Cobalt Complex-Catalyzed Stereodivergent Semireduction of Alkynes: Switchable Selectivities Controlled by H <sub>2</sub> 0. ACS Catalysis, 2021, 11, 13696-13705.	11.2	19
33	A new hybrid observation GNSS tomography method combining the real and virtual inverted signals. Journal of Geodesy, 2021, 95, 1.	3.6	7
34	Highly Regioselective Difluoroalkylarylation of Butadiene through a Nickel-Catalyzed Tandem Radical Process. ACS Catalysis, 2021, 11, 14848-14853.	11.2	12
35	Authentication scheme based on smart card in multi-server environment. Wireless Networks, 2020, 26, 855-863.	3.0	10
36	A new genus and species of sabretooth, <i>Oriensmilus liupanensis</i> (Barbourofelinae, Nimravidae,) Tj ETQqO	0 0 rgBT /0 1.5	Overlock 10 T 12

#	Article	IF	CITATIONS
37	Transformation of Ni-containing birnessite to tectomanganate: Influence and fate of weakly bound Ni(II) species. Geochimica Et Cosmochimica Acta, 2020, 271, 96-115.	3.9	11
38	Coupled morphological and structural evolution of δ-MnO <sub>2</sub> to α-MnO <sub>2</sub> through multistage oriented assembly processes: the role of Mn( <scp>iii</scp> ). Environmental Science: Nano, 2020, 7, 238-249.	4.3	10
39	Realization of an Optimal Dynamic Geodetic Reference Frame in China: Methodology and Applications. Engineering, 2020, 6, 879-897.	6.7	5
40	Oxidation of Mn(III) Species by Pb(IV) Oxide as a Surrogate Oxidant in Aquatic Systems. Environmental Science & Technology, 2020, 54, 14124-14133.	10.0	17
41	An Evaluation of Fengyun-3C Radio Occultation Atmospheric Profiles Over 2015–2018. Remote Sensing, 2020, 12, 2116.	4.0	8
42	Assessments of the Retrieval of Atmospheric Profiles from GNSS Radio Occultation Data in Moist Tropospheric Conditions Using Radiosonde Data. Remote Sensing, 2020, 12, 2717.	4.0	4
43	Node-Based Optimization of GNSS Tomography with a Minimum Bounding Box Algorithm. Remote Sensing, 2020, 12, 2744.	4.0	3
44	A New Four-Layer Inverse Scale Height Grid Model of China for Zenith Tropospheric Delay Correction. IEEE Access, 2020, 8, 210171-210182.	4.2	4
45	Development of an Improved Model for Prediction of Short-Term Heavy Precipitation Based on GNSS-Derived PWV. Remote Sensing, 2020, 12, 4101.	4.0	41
46	The Impact of Different Ocean Tide Loading Models on GNSS Estimated Zenith Tropospheric Delay Using Precise Point Positioning Technique. Remote Sensing, 2020, 12, 3080.	4.0	3
47	Meta-heuristics for unrelated parallel machines scheduling with random rework to minimize expected total weighted tardiness. Computers and Industrial Engineering, 2020, 145, 106505.	6.3	17
48	Molecular Mechanisms of Lead Binding to Ferrihydrite–Bacteria Composites: ITC, XAFS, and μ-XRF Investigations. Environmental Science & Technology, 2020, 54, 4016-4025.	10.0	26
49	Effects of Al substitution on local structure and morphology of lepidocrocite and its phosphate adsorption kinetics. Geochimica Et Cosmochimica Acta, 2020, 276, 109-121.	3.9	27
50	3D Object Recognition and Pose Estimation From Point Cloud Using Stably Observed Point Pair Feature. IEEE Access, 2020, 8, 44335-44345.	4.2	17
51	Formation and transformation of schwertmannite through direct Fe <sup>3+</sup> hydrolysis under various geochemical conditions. Environmental Science: Nano, 2020, 7, 2385-2398.	4.3	14
52	Real-Time GNSS-Derived PWV for Typhoon Characterizations: A Case Study for Super Typhoon Mangkhut in Hong Kong. Remote Sensing, 2020, 12, 104.	4.0	28
53	The Performance of Different Mapping Functions and Gradient Models in the Determination of Slant Tropospheric Delay. Remote Sensing, 2020, 12, 130.	4.0	21
54	Incorporation of Pb( <scp>ii</scp> ) into hematite during ferrihydrite transformation. Environmental Science: Nano, 2020, 7, 829-841.	4.3	16

#	Article	IF	CITATIONS
55	The Speciation of Cd in Cd–Fe Coprecipitates: Does Cd Substitute for Fe in Goethite Structure?. ACS Earth and Space Chemistry, 2019, 3, 2225-2236.	2.7	20
56	Synthesis of Polyethylene with Inâ€Chain α,βâ€Unsaturated Ketone and Isolated Ketone Units: Pdâ€Catalyzed Ringâ€Opening Copolymerization of Cyclopropenone with Ethylene. Angewandte Chemie - International Edition, 2019, 58, 12955-12959.	13.8	30
57	Synthesis of Chiral Tertiary α,αâ€Difluoromethyl Carbinols by Cuâ€Catalyzed Asymmetric Propargylation. Chemistry - A European Journal, 2019, 25, 16425-16434.	3.3	12
58	Synthesis of Polyethylene with Inâ€Chain α,βâ€Unsaturated Ketone and Isolated Ketone Units: Pdâ€Catalyzed Ringâ€Opening Copolymerization of Cyclopropenone with Ethylene. Angewandte Chemie, 2019, 131, 13089-13093.	2.0	7
59	Construction of Allâ€Carbon Chiral Quaternary Centers through Cu <sup>I</sup> â€Catalyzed Enantioselective Reductive Hydroxymethylation of 1,1â€Disubstituted Allenes with CO <sub>2</sub> . Chemistry - A European Journal, 2019, 25, 13874-13878.	3.3	43
60	Modeling of Topside Ionospheric Vertical Scale Height Based on Ionospheric Radio Occultation Measurements. Journal of Geophysical Research: Space Physics, 2019, 124, 4926-4942.	2.4	10
61	Investigation of the performance of real-time BDS-only precise point positioning using the IGS real-time service. GPS Solutions, 2019, 23, 1.	4.3	40
62	Phosphate Sorption Speciation and Precipitation Mechanisms on Amorphous Aluminum Hydroxide. Soil Systems, 2019, 3, 20.	2.6	36
63	Al-substitution-induced defect sites enhance adsorption of Pb <sup>2+</sup> on hematite. Environmental Science: Nano, 2019, 6, 1323-1331.	4.3	26
64	Effects of Mn <sup>2+</sup> , Ni <sup>2+</sup> , and Cu <sup>2+</sup> on the Formation and Transformation of Hydrosulfate Green Rust: Reaction Processes and Underlying Mechanisms. ACS Earth and Space Chemistry, 2019, 3, 519-530.	2.7	14
65	Formation and Morphology Evolution from Ferrihydrite to Hematite in the Presence of Tartaric Acid. ACS Earth and Space Chemistry, 2019, 3, 562-570.	2.7	9
66	Pathogenic CARD11 mutations affect B cell development and differentiation through a noncanonical pathway. Science Immunology, 2019, 4, .	11.9	14
67	Biostratigraphy, magnetostratigraphy, and geochronology of lower Miocene Aoerban strata in Central Inner Mongolia. Palaeogeography, Palaeoclimatology, Palaeoecology, 2019, 518, 187-205.	2.3	8
68	Palladium complexes bearing an Nâ€heterocyclic carbene–sulfonamide ligand for cooligomerization of ethylene and polar monomers. Journal of Polymer Science Part A, 2019, 57, 474-477.	2.3	22
69	Helmert-VCE-aided fast-WTLS approach for global ionospheric VTEC modelling using data from GNSS, satellite altimetry and radio occultation. Journal of Geodesy, 2019, 93, 877-888.	3.6	15
70	Review: Implications of vertebrate fossils for paleo-elevations of the Tibetan Plateau. Global and Planetary Change, 2019, 174, 58-69.	3.5	77
71	Using global navigation satellite system data for real-time moisture analysis and forecasting over the Australian region I. The system. Journal of Southern Hemisphere Earth Systems Science, 2019, 69, 161.	1.8	7
72	Unprecedented Dearomatized Spirocyclopropane in a Sequential Rhodium(III) atalyzed Câ^'H Activation and Rearrangement Reaction. Angewandte Chemie - International Edition, 2018, 57, 5520-5524.	13.8	42

#	Article	IF	CITATIONS
73	Effiziente Synthese von arylierten Furanen durch sequentielle Rhodiumâ€katalysierte Arylierung und Cycloisomerisierung von Cyclopropenen. Angewandte Chemie, 2018, 130, 1728-1732.	2.0	18
74	Uhrf1 regulates germinal center B cell expansion and affinity maturation to control viral infection. Journal of Experimental Medicine, 2018, 215, 1437-1448.	8.5	30
75	Beispielloses dearomatisiertes Spirocyclopropan in einer sequenziellen Rhodium(III)â€katalysierten Câ€Hâ€Aktivierung und Umlagerungsreaktion. Angewandte Chemie, 2018, 130, 5618-5622.	2.0	11
76	Notes on the origin of extensive endorheic regions in central and northern Mexico, and some implications for paleozoogeography. Journal of South American Earth Sciences, 2018, 83, 55-67.	1.4	8
77	Efficient Synthesis of Arylated Furans by a Sequential Rhâ€Catalyzed Arylation and Cycloisomerization of Cyclopropenes. Angewandte Chemie - International Edition, 2018, 57, 1712-1716.	13.8	77
78	Fossil canids from the Mehrten Formation, Late Cenozoic of Northern California. Journal of Vertebrate Paleontology, 2018, 38, e1405009.	1.0	4
79	A new otter of giant size, <i>Siamogale melilutra</i> sp. nov. (Lutrinae: Mustelidae: Carnivora), from the latest Miocene Shuitangba site in north-eastern Yunnan, south-western China, and a total-evidence phylogeny of lutrines. Journal of Systematic Palaeontology, 2018, 16, 39-65.	1.5	31
80	Photosynthetic pathway of grass fossils from the upper Miocene Dove Spring Formation, Mojave Desert, California. Palaeogeography, Palaeoclimatology, Palaeoecology, 2018, 490, 131-140.	2.3	3
81	Design, synthesis, biological evaluation and cocrystal structures with tubulin of chiral β -lactam bridged combretastatin A-4 analogues as potent antitumor agents. European Journal of Medicinal Chemistry, 2018, 144, 817-842.	5.5	50
82	Improvement of Reflection Detection Success Rate of GNSS RO Measurements Using Artificial Neural Network. IEEE Transactions on Geoscience and Remote Sensing, 2018, 56, 760-769.	6.3	8
83	Plausible Rh(V) Intermediates in Catalytic C–H Activation Reactions. ACS Catalysis, 2018, 8, 242-257.	11.2	134
84	A new approach for GNSS tomography from a few GNSS stations. Atmospheric Measurement Techniques, 2018, 11, 3511-3522.	3.1	9
85	Selective Chain-End Functionalization of Polar Polyethylenes: Orthogonal Reactivity of Carbene and Polar Vinyl Monomers in Their Copolymerization with Ethylene. Journal of the American Chemical Society, 2018, 140, 15635-15640.	13.7	52
86	Methyltransferase Nsd2 Ensures Germinal Center Selection by Promoting Adhesive Interactions between B Cells and Follicular Dendritic Cells. Cell Reports, 2018, 25, 3393-3404.e6.	6.4	13
87	Catalytic enantioselective synthesis of cyclopropanes featuring vicinal all-carbon quaternary stereocenters with a CH <sub>2</sub> F group; study of the influence of C–Fâ√H–N interactions on reactivity. Organic Chemistry Frontiers, 2018, 5, 2960-2968.	4.5	30
88	The correlation between GNSS-derived precipitable water vapor and sea surface temperature and its responses to El Niño–Southern Oscillation. Remote Sensing of Environment, 2018, 216, 1-12.	11.0	74
89	Making Spiroketalâ€based Diphosphine (SKP) Ligands via a Catalytic Asymmetric Approach. Chinese Journal of Chemistry, 2018, 36, 899-903.	4.9	25
90	Assessment of Multiple GNSS Real-Time SSR Products from Different Analysis Centers. ISPRS International Journal of Geo-Information, 2018, 7, 85.	2.9	69

#	Article	IF	CITATIONS
91	Magnetostratigraphic dating of the late Miocene Baogeda Ula Formation and associated fauna in central Inner Mongolia, northern China. Palaeogeography, Palaeoclimatology, Palaeoecology, 2018, 505, 243-255.	2.3	5
92	First bone-cracking dog coprolites provide new insight into bone consumption in Borophagus and their unique ecological niche. ELife, 2018, 7, .	6.0	12
93	Cp*Rh(III)/Bicyclic Olefin Cocatalyzed C–H Bond Amidation by Intramolecular Amide Transfer. Journal of the American Chemical Society, 2017, 139, 6506-6512.	13.7	107
94	Lis1 Regulates Germinal Center B Cell Antigen Acquisition and Affinity Maturation. Journal of Immunology, 2017, 198, 4304-4311.	0.8	8
95	Palladium-catalyzed asymmetric allylic amination: enantioselective synthesis of chiral α-methylene substituted β-aminophosphonates. Organic Chemistry Frontiers, 2017, 4, 271-276.	4.5	32
96	Discovery of the fossil otter Enhydritherium terraenovae (Carnivora, Mammalia) in Mexico reconciles a palaeozoogeographic mystery. Biology Letters, 2017, 13, 20170259.	2.3	4
97	Palladiumâ€Catalyzed Asymmetric Construction of Vicinal Tertiary and Allâ€Carbon Quaternary Stereocenters by Allylation of βâ€Ketocarbonyls with Morita–Baylis–Hillman Adducts. Angewandte Chemie - International Edition, 2017, 56, 5050-5054.	13.8	79
98	Palladium atalyzed Asymmetric Construction of Vicinal Tertiary and All arbon Quaternary Stereocenters by Allylation of βâ€Ketocarbonyls with Morita–Baylis–Hillman Adducts. Angewandte Chemie, 2017, 129, 5132-5136.	2.0	20
99	Pieces of the puzzle: Lack of significant C4 in the late Miocene of southern California. Palaeogeography, Palaeoclimatology, Palaeoecology, 2017, 475, 70-79.	2.3	9
100	Palladium atalyzed Asymmetric Allylic Allylation of Racemic Morita–Baylis–Hillman Adducts. Angewandte Chemie, 2017, 129, 1136-1139.	2.0	14
101	Palladium atalyzed Asymmetric Allylic Allylation of Racemic Morita–Baylis–Hillman Adducts. Angewandte Chemie - International Edition, 2017, 56, 1116-1119.	13.8	66
102	Combination of Cp*Rh <sup>III</sup> â€Catalyzed Câ^'H Activation and a Wagner–Meerweinâ€Type Rearrangement. Angewandte Chemie - International Edition, 2017, 56, 1381-1384.	13.8	83
103	Phosphate and phytate adsorption and precipitation on ferrihydrite surfaces. Environmental Science: Nano, 2017, 4, 2193-2204.	4.3	81
104	Kombination von Cp*Rh III â€katalysierter Câ€Hâ€Aktivierung mit einer Variante der Wagnerâ€Meerweinâ€Umlagerung. Angewandte Chemie, 2017, 129, 1401-1405.	2.0	21
105	Feeding capability in the extinct giant Siamogale melilutra and comparative mandibular biomechanics of living Lutrinae. Scientific Reports, 2017, 7, 15225.	3.3	17
106	A basal ursine bear (Protarctos abstrusus) from the Pliocene High Arctic reveals Eurasian affinities and a diet rich in fermentable sugars. Scientific Reports, 2017, 7, 17722.	3.3	22
107	Seasonal Multifactor Modelling of Weighted-Mean Temperature for Ground-Based GNSS Meteorology in Hunan, China. Advances in Meteorology, 2017, 2017, 1-13.	1.6	11
108	Revocable Key-Aggregate Cryptosystem for Data Sharing in Cloud. Security and Communication Networks, 2017, 2017, 1-11.	1.5	10

#	Article	IF	CITATIONS
109	A new voxel-based model for the determination of atmospheric weighted mean temperature in GPS atmospheric sounding. Atmospheric Measurement Techniques, 2017, 10, 2045-2060.	3.1	38
110	Determination of zenith hydrostatic delay and its impact on GNSS-derived integrated water vapor. Atmospheric Measurement Techniques, 2017, 10, 2807-2820.	3.1	45
111	Public Key Encryption with Keyword Search from Lattices in Multiuser Environments. Mathematical Problems in Engineering, 2016, 2016, 1-7.	1.1	2
112	Water vaporâ€weighted mean temperature and its impact on the determination of precipitable water vapor and its linear trend. Journal of Geophysical Research D: Atmospheres, 2016, 121, 833-852.	3.3	127
113	An enhanced singular spectrum analysis method for constructing nonsecular model of GPS site movement. Journal of Geophysical Research: Solid Earth, 2016, 121, 2193-2211.	3.4	28
114	Out of Tibet: an early sheep from the Pliocene of Tibet, <i>Protovis himalayensis</i> , genus and species nov. (Bovidae, Caprini), and origin of Ice Age mountain sheep. Journal of Vertebrate Paleontology, 2016, 36, e1169190.	1.0	21
115	A Comparative Investigation: Group 9 Cp*M(III)-Catalyzed Formal [4Â+ 2] Cycloaddition as an Atom-Economic Approach to Quinazolines. Organic Letters, 2016, 18, 2090-2093.	4.6	143
116	Highly selective synthesis of 6-substituted benzothiophenes by Sc(OTf) <sub>3</sub> -catalyzed intermolecular cyclization and sulfur migration. Organic Chemistry Frontiers, 2016, 3, 1619-1623.	4.5	22
117	The Late Miocene <i>Hipparion</i> (Equidae, Perissodactyla) fossils from Baogeda Ula, Inner Mongolia, China. Historical Biology, 2016, 28, 53-68.	1.4	6
118	Pliocene bone-cracking Hyaeninae (Carnivora, Mammalia) from the Zanda Basin, Tibet Autonomous Region, China. Historical Biology, 2016, 28, 69-77.	1.4	8
119	Contributions to vertebrate palaeontology in honour of Yukimitsu Tomida. Historical Biology, 2016, 28, 1-7.	1.4	2
120	Cp*Rh <sup>III</sup> atalyzed Arylation of C(sp <sup>3</sup> )ï£;H Bonds. Angewandte Chemie - International Edition, 2015, 54, 10280-10283.	13.8	86
121	Approximation algorithms for the three-stage flexible flow shop problem with mid group constraint. Expert Systems With Applications, 2015, 42, 3571-3584.	7.6	8
122	Proactive approach for stochastic RCMPSP based on multi-priority rule combinations. International Journal of Production Research, 2015, 53, 1098-1110.	7.5	24
123	Highly Regio- and Enantioselective Alkoxycarbonylative Amination of Terminal Allenes Catalyzed by a Spiroketal-Based Diphosphine/Pd(II) Complex. Journal of the American Chemical Society, 2015, 137, 15346-15349.	13.7	88
124	Earliest record of Sinicuon in Zanda Basin, southern Tibet and implications for hypercarnivores in cold environments. Quaternary International, 2015, 355, 3-10.	1.5	21
125	Cenozoic vertebrate evolution and paleoenvironment in Tibetan Plateau: Progress and prospects. Gondwana Research, 2015, 27, 1335-1354.	6.0	54
126	Into Tibet: An Early Pliocene Dispersal of Fossil Zokor (Rodentia: Spalacidae) from Mongolian Plateau to the Hinterland of Tibetan Plateau. PLoS ONE, 2015, 10, e0144993.	2.5	18

#	Article	IF	CITATIONS
127	A transitional skunk, <i>Buisnictis metabatos</i> sp. nov. (Mephitidae, Carnivora), from Baja California Sur and the role of southern refugia in skunk evolution. Journal of Systematic Palaeontology, 2014, 12, 291-302.	1.5	6
128	Himalayan fossils of the oldest known pantherine establish ancient origin of big cats. Proceedings of the Royal Society B: Biological Sciences, 2014, 281, 20132686.	2.6	68
129	Spiroketal-Based Diphosphine Ligands in Pd-Catalyzed Asymmetric Allylic Amination of Morita–Baylis–Hillman Adducts: Exceptionally High Efficiency and New Mechanism. Journal of the American Chemical Society, 2014, 136, 405-411.	13.7	133
130	Numerical Simulation and Forecasting of Water Level for Qinghai Lake Using Multi-Altimeter Data Between 2002 and 2012. IEEE Journal of Selected Topics in Applied Earth Observations and Remote Sensing, 2014, 7, 609-622.	4.9	18
131	Vertebrate fossils on the roof of the world: Biostratigraphy and geochronology of high-elevation Kunlun Pass Basin, northern Tibetan Plateau, and basin history as related to the Kunlun strike-slip fault. Palaeogeography, Palaeoclimatology, Palaeoecology, 2014, 411, 46-55.	2.3	21
132	From †third pole' to north pole: a Himalayan origin for the arctic fox. Proceedings of the Royal Society B: Biological Sciences, 2014, 281, 20140893.	2.6	55
133	Estimation of Mold Remaining Duration Considering Reworks. Jixie Gongcheng Xuebao/Chinese Journal of Mechanical Engineering, 2014, 50, 199.	0.5	0
134	Scheduling rules for two-stage flexible flow shop scheduling problem subject to tail group constraint. International Journal of Production Economics, 2013, 146, 667-678.	8.9	15
135	A new cursorial hyena from Tibet, and analysis of biostratigraphy, paleozoogeography, and dental morphology of <i>Chasmaporthetes</i> (Mammalia, Carnivora). Journal of Vertebrate Paleontology, 2013, 33, 1457-1471.	1.0	33
136	Practical Asymmetric Catalytic Synthesis of Spiroketals and Chiral Diphosphine Ligands. Advanced Synthesis and Catalysis, 2013, 355, 2900-2907.	4.3	63
137	Mio-Pleistocene Zanda Basin biostratigraphy and geochronology, pre-Ice Age fauna, and mammalian evolution in western Himalaya. Palaeogeography, Palaeoclimatology, Palaeoecology, 2013, 374, 81-95.	2.3	47
138	Diet and environment of a mid-Pliocene fauna from southwestern Himalaya: Paleo-elevation implications. Earth and Planetary Science Letters, 2013, 376, 43-53.	4.4	40
139	Mortgaging the future of chinese paleontology. Proceedings of the National Academy of Sciences of the United States of America, 2013, 110, 3201-3201.	7.1	6
140	Highly Stereoselective Olefin Cyclopropanation of Diazooxindoles Catalyzed by a <i>C</i> <sub>2</sub> -Symmetric Spiroketal Bisphosphine/Au(I) Complex. Journal of the American Chemical Society, 2013, 135, 8197-8200.	13.7	318
141	Oligocene-Miocene Mammalian Fossils from Hongyazi Basin and Its Bearing on Tectonics of Danghe Nanshan in Northern Tibetan Plateau. PLoS ONE, 2013, 8, e82816.	2.5	8
142	Locomotive implication of a Pliocene three-toed horse skeleton from Tibet and its paleo-altimetry significance. Proceedings of the National Academy of Sciences of the United States of America, 2012, 109, 7374-7378.	7.1	51
143	Late Neogene environmental changes in the central Himalaya related to tectonic uplift and orbital forcing. Journal of Asian Earth Sciences, 2012, 44, 62-76.	2.3	29
144	Diets and environments of late Cenozoic mammals in the Qaidam Basin, Tibetan Plateau: Evidence from stable isotopes. Earth and Planetary Science Letters, 2012, 333-334, 70-82.	4.4	50

#	Article	IF	CITATIONS
145	Aromatic Spiroketal Bisphosphine Ligands: Palladiumâ€Catalyzed Asymmetric Allylic Amination of Racemic Morita–Baylis–Hillman Adducts. Angewandte Chemie - International Edition, 2012, 51, 9276-9282.	13.8	186
146	Catalytic Asymmetric Synthesis of Aromatic Spiroketals by SpinPhox/Iridium(I)â€Catalyzed Hydrogenation and Spiroketalization of α,α′â€Bis(2â€hydroxyarylidene) Ketones. Angewandte Chemie - International Edition, 2012, 51, 936-940.	13.8	228
147	Do convergent ecomorphs evolve through convergent morphological pathways? Cranial shape evolution in fossil hyaenids and borophagine canids (Carnivora, Mammalia). Paleobiology, 2011, 37, 470-489.	2.0	25
148	Out of Tibet: Pliocene Woolly Rhino Suggests High-Plateau Origin of Ice Age Megaherbivores. Science, 2011, 333, 1285-1288.	12.6	164
149	Model Sensitivity and Use of the Comparative Finite Element Method in Mammalian Jaw Mechanics: Mandible Performance in the Gray Wolf. PLoS ONE, 2011, 6, e19171.	2.5	32
150	Discovery of the upper dentition of <i>Barbourofelis whitfordi</i> (Nimravidae, Carnivora) and an evaluation of the genus in California. Journal of Vertebrate Paleontology, 2010, 30, 244-254.	1.0	10
151	Cranial functional morphology of fossil dogs and adaptation for durophagy in <i>Borophagus</i> and <i>Epicyon</i> (Carnivora, Mammalia). Journal of Morphology, 2010, 271, 1386-1398.	1.2	53
152	A new species of crown-antlered deerStephanocemas(Artiodactyla, Cervidae) from the middle Miocene of Qaidam Basin, northern Tibetan Plateau, China, and a preliminary evaluation of its phylogeny. Zoological Journal of the Linnean Society, 2009, 156, 680-695.	2.3	14
153	C4 expansion in the central Inner Mongolia during the latest Miocene and early Pliocene. Earth and Planetary Science Letters, 2009, 287, 311-319.	4.4	57
154	Earliest hog-nosed skunk, <i>Conepatus</i> (Mephitidae, Carnivora), from the early Pliocene of Guanajuato, Mexico and origin of South American skunks. Zoological Journal of the Linnean Society, 2008, 154, 386-407.	2.3	23
155	Stable isotopes in fossil mammals, fish and shells from Kunlun Pass Basin, Tibetan Plateau: Paleo-climatic and paleo-elevation implications. Earth and Planetary Science Letters, 2008, 270, 73-85.	4.4	72
156	Extraordinarily thick-boned fish linked to the aridification of the Qaidam Basin (northern Tibetan) Tj ETQq0 0 0 rgB 13246-13251.	T /Overloc 7.1	ck 10 Tf 50 61
157	The first record of the late Miocene <i>Hyaenictitherium hyaenoides</i> Zdansky (Carnivora: Hyaenidae) in Inner Mongolia and an evaluation of the genus. Journal of Vertebrate Paleontology, 2007, 27, 699-708.	1.0	13
158	Vertebrate paleontology, biostratigraphy, geochronology, and paleoenvironment of Qaidam Basin in northern Tibetan Plateau. Palaeogeography, Palaeoclimatology, Palaeoecology, 2007, 254, 363-385.	2.3	139
159	High-resolution magnetostratigraphy of the Neogene Huaitoutala section in the eastern Qaidam Basin on the NE Tibetan Plateau, Qinghai Province, China and its implication on tectonic uplift of the NE Tibetan Plateau. Earth and Planetary Science Letters, 2007, 258, 293-306.	4.4	439
160	A new basal skunkMartinogale(Carnivora, Mephitinae) from Late Miocene Dove Spring Formation, California, and origin of New World mephitines. Journal of Vertebrate Paleontology, 2005, 25, 936-949.	1.0	22
161	Microstructural Reinforcement in the Canine Enamel of the Hyaenid Crocuta crocuta, the FelidPuma concolorand the Late Miocene Canid Borophagus secundus. Journal of Mammalian Evolution, 2005, 12, 379-403.	1.8	15
162	Amphicticeps and Amphicynodon (Arctoidea, Carnivora) from Hsanda Gol Formation, Central Mongolia and Phylogeny of Basal Arctoids with Comments on Zoogeography. American Museum Novitates, 2005, 3483, 1-60.	0.6	71

#	Article	IF	CITATIONS
163	A new leptarctine (Carnivora: Mustelidae) from the early Miocene of the northern Tibetan Plateau: implications for the phylogeny and zoogeography of basal mustelids. Zoological Journal of the Linnean Society, 2004, 142, 405-421.	2.3	24
164	Two new carnivores from an unusual late Tertiary forest biota in eastern North America. Nature, 2004, 431, 556-559.	27.8	85
165	Late MiocenePromephitis(Carnivora, Mephitidae) from China. Journal of Vertebrate Paleontology, 2004, 24, 721-731.	1.0	21
166	A new species ofAelurodon(Carnivora, Canidae) from the Barstovian of Montana. Journal of Vertebrate Paleontology, 2004, 24, 445-452.	1.0	5
167	Cope's Rule, Hypercarnivory, and Extinction in North American Canids. Science, 2004, 306, 101-104.	12.6	281
168	Danghe area (western Gansu, China) biostratigraphy and implications for depositional history and tectonics of northern Tibetan Plateau. Earth and Planetary Science Letters, 2003, 208, 253-269.	4.4	107
169	Didymoconus(Mammalia: Didymoconidae) from Lanzhou Basin, China and its stratigraphic and ecological significance. Journal of Vertebrate Paleontology, 2001, 21, 555-564.	1.0	6
170	New cranial material of <i>Simocyon</i> from China, and its implications for phylogenetic relationship to the red panda <i>(Ailurus)</i> . Journal of Vertebrate Paleontology, 1997, 17, 184-198.	1.0	44
171	Carnilestes, A New Primitive Lipotyphlan (Insectivora: Mammalia) From the Early and Middle Paleocene, Nanxiong Basin, China. Journal of Vertebrate Paleontology, 1995, 15, 131-145.	1.0	11
172	Multiple hereditary osteochondroma in OligoceneHesperocyon(Carnivora: Canidae). Journal of Vertebrate Paleontology, 1992, 12, 387-394.	1.0	40
173	The status of genusNothocyonMatthew, 1899 (Carnivora): an arctoid not a canid. Journal of Vertebrate Paleontology, 1992, 12, 223-229.	1.0	7
174	Sonitictis moralesi, gen. et sp. nov, a new hypercarnivorous and durophagous mustelid from middle Miocene Tunggur Formation, Inner Mongolia, China and its functional morphology. Historical Biology, 0, , 1-12.	1.4	0
175	Deoxygenative Cross oupling of Aromatic Amides with Polyfluoroarenes. Angewandte Chemie, 0, , .	2.0	2
176	Fast spread followed by anagenetic evolution in Eurasian and North American <i>Amphimachairodus</i> . Historical Biology, 0, , 1-19.	1.4	1
177	Markovnikovâ€5elective Hydroboration of Aryl Alkenes Enabled by A Simple Nickel Salt. Chinese Journal of Chemistry, 0, , .	4.9	3